

Dominant formation and quenching processes in E -beam pumped ArF^* and KrF^* lasers[†]

M. Rokni,[‡] J. H. Jacob, and J. A. Mangano

Avco Everett Research Laboratory, Inc., Everett, Massachusetts 02149

(Received 7 July 1977)

The dominant formation and quenching processes in E -beam pumped ArF^* and KrF^* lasers are discussed. The quenching of ArF^* by F_2 and Ar has been measured by analyzing the ArF^* ($B^2\Sigma_{1/2} \rightarrow X^2\Sigma_{1/2}$) fluorescence as a function of the F_2 and Ar partial pressures. We have also measured the displacement of the Ar in ArF^* by Kr to form KrF^* . The dominant quenching processes of KrF^* were identified, and the rate constants were measured. The ArF^* and KrF^* are formed from the ionic states with high efficiency. Interception of the precursors can be made negligible by choosing the experimental conditions properly. The quenching of KrF^* by Ar and Kr is mainly a three-body process resulting in the formation of Kr_2F^* . The emission from Kr_2F^* was observed in a broadband centered at 410 nm. We have verified that the Kr_2F^* is produced subsequent to the KrF^* formation by performing a laser saturation experiment.

I. INTRODUCTION

Much research has been performed on the rare-gas monohalide exciplexes¹ since their spectra were first reported by Velazco and Setser.² In the two years following the Velazco-Setser publication, many of these molecules have been made to lase by both pure E -beam³ and discharge pumping.⁴ The most promising candidates that are scalable to high output power and efficiency are the rare-gas fluorides.^{5,6} To facilitate the scaling of these lasers to high average power, a detailed knowledge of the kinetic processes is necessary. Velazco, Kolts, and Setser⁷ have shown that the rare-gas fluorides are formed with high efficiency from excited rare gases. We will show that the rare-gas ions also produce these exciplex species with high efficiency. The formation rate of these excited molecules is rapid since they can be accessed through an ion channel: E -beam ionization of the rare gas followed by rapid dissociative electron attachment to the halogen and subsequent extremely rapid ion-ion recombination.

In this paper we will discuss the formation and quenching of the ArF^* and KrF^* exciplexes. The kinetic processes were investigated by irradiating mixtures of rare gases and fluorine by a beam of fast electrons. The fluorescence emanating from these mixes was monitored and recorded. The kinetic processes were isolated by studying the dependence of the fluorescence on the partial pressure of one of the constituents of the gas mixture, while the partial pressures of the remaining gases in the mixture were kept constant. By analyzing the dependence of the quasi-steady-state fluorescence on the partial pressures of the rare gases and fluorine and the power deposited into the gas mixture, we obtained the various quenching-rate constants. It should be noted that only relative

intensity measurements were required by the analysis.⁸

Section II presents a discussion of the experimental apparatus used to make the measurements. The formation and quenching processes in ArF^* are presented and discussed in Sec. III. A similar presentation for KrF^* is made in Sec. IV.

II. EXPERIMENTAL SETUP

The experimental setup is shown schematically in Fig. 1. The gas mixtures were excited by a high-energy E beam. The electrons were generated from a cold cathode and accelerated to an energy of 150 keV in a vacuum chamber at a background pressure of $\leq 10^{-5}$ torr. The fast electrons

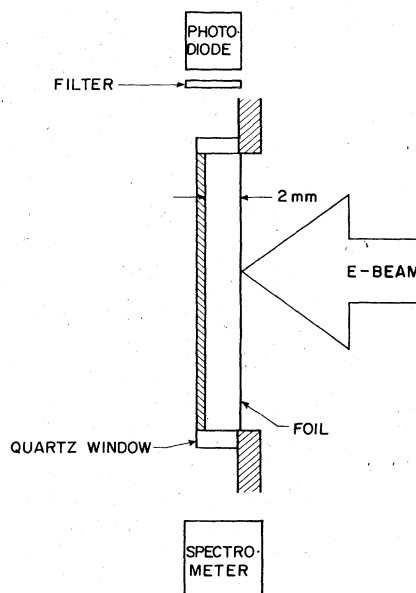


FIG. 1. Schematic of experimental set-up.

passed through a 2-mil Kapton foil that separated the gas mixture from the high-vacuum chamber containing the cold cathode. The mixture was contained in a teflon cell with dimensions $22 \times 2 \times 0.2$ cm³. The dimension of the cell along the initial *E*-beam direction was 0.2 cm to ensure uniform energy deposition by the *E* beam up to mixture pressures of 4 atm. The *E*-beam current density, after attenuation by the foil and supporting structure, was 5 A/cm². The current density could be further attenuated by introducing a partially transmitting screen on the high-vacuum side of the foil. The *E*-beam pulse length was 300 nsec long, enabling the fluorescence amplitude to reach a steady state.

The fluorescence intensities were monitored by appropriate filters and photodiodes, and spectra were recorded on a 1-m Hilger spectrograph. In the case of the ArF* radiation, the side of the filter facing the photodiode was coated with sodium salicylate. The sodium salicylate converts the 193 nm photons into visible and near-uv radiation. Care was taken to ensure that the spectral width of the filters were large enough so that the transmitted radiation was representative of the overall kinetic processes.

The gases were premixed in a Teflon-coated stainless steel tank. Adequate time was allowed to ensure complete diffusive mixing. The gas mixtures were introduced into the Teflon cell, which could be evacuated to pressures of $\leq 10^{-4}$ torr. Research-grade (Matheson) Ar and Xe were used without any further purification. The gases were analyzed by Gollob Analytical Service, Inc., and found to have less than 100 ppm of O₂, N₂, H₂O, and CO₂ impurities. The F₂ was 98% pure.

III. FORMATION AND QUENCHING OF ArF*

Since Ar is the main constituent in most rare-gas fluoride laser mixes, most of the *E*-beam energy is deposited in the argon. So it is reasonable to first investigate the kinetic processes in *E*-beam pumped Ar/F₂ mixes.

A. Formation of ArF*

Table I lists the dominant formation kinetics for low-current-density (≤ 10 A/cm²) *E*-beam pumped systems. About 55% of the *E*-beam energy deposited in the gas is channeled into Ar⁺ formation as given by reaction (1). Approximately 10% of the deposited energy is channeled into Ar* formation by the energetic secondary electrons formed in reaction (1).⁹

For our experimental conditions, i.e., Ar pressures below 4 atm, mixtures containing ≥ 2 torr of F₂ and *E*-beam currents ≤ 5 A/cm², the main loss mechanism for secondary electrons is dissociative attachment by F₂ resulting in the formation of F⁻. Hence the dominant ArF* formation mechanism proceeds via the ion channel¹⁰ [see reactions (4) and (7) in Table I]. If the pump power or pressure stated above are exceeded, dissociative recombination of *e*_s with Ar₂⁺ (*e*_s + Ar₂⁺ → Ar* + Ar) becomes important. The exciplex formation will then proceed via the metastable channel (reaction 5, Table I). When the exciplex formation proceeds via the metastables, losses due to Penning ionization (Ar* + Ar* → Ar⁺ + *e*_s + Ar) and rare-gas excimer formation (Ar₂^{*}) must be considered. Figure 2 shows the variation of *e*_s, F⁻, Ar⁺, and Ar₂⁺ for a mixture

TABLE I. Dominant formation kinetics for ArF*.

$\bar{e} + \text{Ar} \rightarrow \text{Ar}^+ + \bar{e} + e_s$	26.4 eV/ion pair ^a	(1)
$e_s + \text{F}_2 \rightarrow \text{F}^- + \text{F}$	5×10^{-9} cm ³ /sec ^b	(2)
$e_s + \text{Ar} \rightarrow \text{Ar}^* + e_s^c$		(3)
$\text{F}^- + \text{Ar}^+ + (M) \rightarrow \text{ArF}^* + (M)$	$10^{-7} + 10^{-7} p$, $p < 1$ atm	(4)
$\text{Ar}^* + \text{F}_2 \rightarrow \text{ArF}^* + \text{F}$	7.5×10^{-10} cm ³ /sec ^d	(5)
Pressure > 1 atm		
$\text{Ar}^+ + \text{F}^- + (M) \rightarrow \text{ArF}^* + (M)$	1.1×10^{-6} cm ³ /sec	(4a)
$\text{Ar}^+ + 2\text{Ar} \rightarrow \text{Ar}_2^+ + \text{Ar}$	2.5×10^{-31} cm ⁶ /sec ^e	(6)
$\text{Ar}_2^+ + \text{F}^- \rightarrow \text{ArF}^* + \text{Ar}$	1.1×10^{-6} cm ³ /sec ^f	(7)

^aSee, for example, U. Fano, Ann. Rev. Sci. **13**, 54 (1963).

^bReference 21.

^cAbout 10% of the *E*-beam power deposited in the gas results in metastable formation (Ref. 9).

^dReference 7.

^eReference 22.

^fIn the numerical results presented we have assumed that the rate constants for reactions (4a) and (7) are the same.

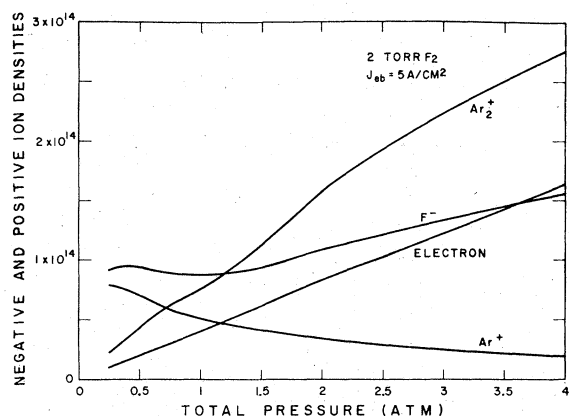


FIG. 2. Calculated densities of e_s , Ar^+ , Ar_2^+ , and F^- as a function of pressure in a Ar/F_2 mixture containing 2-torr F_2 .

containing 2 torr of F_2 plus Ar. The Ar_2^+ and Ar^+ densities are nearly equal at 1 atm. At 4 atm the electron density is slightly greater than the F^- density. Even at these high pressures only 20% of the ArF^* formation proceeds via the electron recombination channel.

At pressures below 1 atm, ArF^* is mainly formed via reaction (4). In this pressure range the ion equivalent two-body recombination-rate constant increases linearly with pressure (three-body process). This three-body reaction becomes diffusion limited at pressures >1 atm. Between pressures of 1–4 atm, this reaction is expected to reach an effective two-body rate of $\sim 10^{-6}$ cm^3/sec .¹¹ At pressures ≈ 1 atm, Ar_2^+ and Ar^+ have almost the same number densities. Ar_2^+ recombines with F^- via a two-body reaction to form ArF^* [reaction (7)]. The molecular ions could possibly form Ar_2F^* via $\text{Ar}_2^+ + \text{F}^- + M \rightarrow \text{Ar}_2\text{F}^* + M$. However, it will be shown subsequently that this process is unimportant. Once ArF^* is formed, it can radiate or be quenched by F_2 or other constituents of the gas mixture. The dominant quenching processes and measured rate constants are listed in Table II.

B. Quenching of ArF^*

A series of experiments were run with 2 torr of F_2 and varying Ar pressure from 60 torr to 1 atm.

The signal increased linearly to about 200 torr of Ar. As the E -beam power deposited into the mix increases linearly with Ar partial pressure, this result shows that Ar quenching of ArF^* is negligibly small at partial pressures of ≤ 200 torr.

We next observed the ArF^* fluorescence keeping the Ar partial pressure fixed at 150 torr¹² and varying the F_2 partial pressure from 2–20 torr. A Stern-Volmer plot of the ArF^* fluorescence data as a function of the F_2 partial pressure is shown in Fig. 3. From this plot, the half-pressure for F_2 , i.e., the pressure of F_2 where the inverse quenching rate becomes equal to ArF^* lifetime, is 4.0 torr.

To determine the quenching of ArF^* by Ar, experiments were performed keeping the partial pressure of F_2 fixed at 2 torr and varying the partial pressure of Ar from 100 torr to 4 atm. Figure 4 shows the data for a typical set of runs. Notice that the signal increases up to a pressure of about 1 atm and then decreases slowly.

There are two possibilities for the observed decay: (i) ArF^* quenching by Ar in two- and three-body processes or (ii) decreasing formation efficiency of ArF^* . As the Ar pressure is increased, reaction (6) (in Table I) occurs more frequently to form molecular ions Ar_2^+ . In fact, from Fig. 2, we see that at the highest pressure the density of Ar_2^+ is ten times that of Ar^+ . These molecular ions will recombine with F^- and can form ArF^* or possibly the excited triatomic Ar_2F^* . The formation of the Ar_2F^* by this channel will result in a smaller formation efficiency of ArF^* and could account for the observed decrease in the fluorescence with increasing pressure. To ensure that this was not the case, we attenuated the E -beam current by a factor of 25. This causes a decrease of the F^- density by at least a factor of 5, resulting in a higher probability of Ar_2^+ formation at a given pressure. So changing the current by a factor of 25 should affect the fluorescence efficiency of ArF^* if $\text{Ar}_2^+ + \text{F}^-$ forms Ar_2F^* . Figure 5 shows the experimentally determined ratio of the ArF^* fluorescence intensity as a function of pressure when the E -beam current is changed by a factor of 25. Also shown are predicted ratios for

TABLE II. Dominant quenching processes of ArF^* .

Reaction	Rate constant $\times \text{ArF}^*$ lifetime	Rate constant ^a
$\text{ArF}^* + \text{F}_2 \rightarrow \text{Products}$	$7.6 \pm 0.7 \times 10^{-18} \text{ cm}^3$	$1.9 \times 10^{-9} \text{ cm}^3/\text{sec}$
$\text{ArF}^* + \text{Kr} \rightarrow \text{KrF}^* + \text{Ar}$	$6.1 \pm 0.5 \times 10^{-18} \text{ cm}^3$	$1.6 \times 10^{-9} \text{ cm}^3/\text{sec}$
$\text{ArF}^* + \text{Ar} \rightarrow \text{Products}$	$3.6 \pm 1 \times 10^{-20} \text{ cm}^3$	$9 \times 10^{-12} \text{ cm}^3/\text{sec}$
$\text{ArF}^* + 2\text{Ar} \rightarrow \text{Ar}_2\text{F}^* + \text{Ar}$	$1.6 \pm 0.3 \times 10^{-39} \text{ cm}^6$	$4 \times 10^{-31} \text{ cm}^6/\text{sec}$

^aThe rate constants have been evaluated assuming an ArF^* lifetime of 4 nsec (Ref. 10).

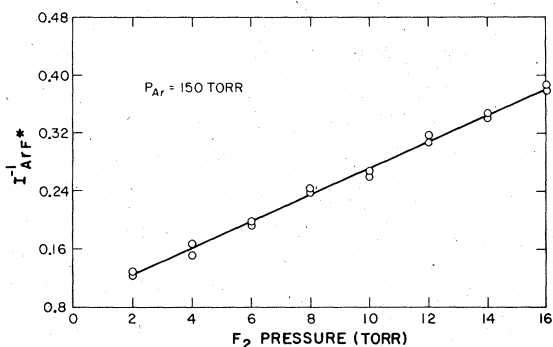


FIG. 3. Stern-Volmer quenching curve for $\text{ArF}^*(^2\Sigma_{1/2})$ with F_2 .

three cases: (i) 100% of Ar_2^+ forms ArF^* , (ii) 80% of Ar_2^+ forms ArF^* , and (iii) 60% of Ar_2^+ forms ArF^* . From Fig. 5 we can conclude that almost all the Ar_2^+ forms ArF^* . Note that as the fraction of Ar_2^+ that forms ArF^* decreases, the predicted ratio of the fluorescence intensities becomes larger than the ratio of the corresponding E -beam currents (25). This is because for branching ratios <1 ,¹³ losses resulting from Ar_2^+ formation become more important as the current is decreased. The results in Fig. 5 prove that the dominant product of $\text{Ar}_2^+ + \text{F}^-$ recombination is ArF^* and not Ar_2F^* . Recent *ab initio* calculations by Wadt and Hay¹⁴ show that the stable configuration of Ar_2F^* is triangular. So for $\text{Ar}_2^+ + \text{F}^-$ to form Ar_2F^* , the F^- ion trajectory has to be contained in the plane that is normal to the axis of symmetry. Any other trajectory will result in a strong interaction between the F^- and Ar^+ and reduce the attractive force between the Ar^+ and Ar resulting in ArF^* formation.

As a result of the experimental results and calculations shown in Fig. 5, one can conclude that the decrease in the fluorescence amplitude with

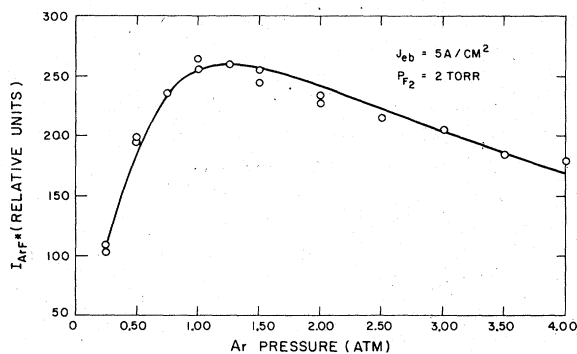


FIG. 4. $\text{ArF}^*(^2\Sigma_{1/2} \rightarrow ^2\Sigma_{1/2})$ fluorescence in the presence of 2-torr F_2 as a function of Ar partial pressure. The points are experimental values for 5 A/cm² E -beam current. The curve is the expected ArF^* fluorescence using the measured quenching rate constants.

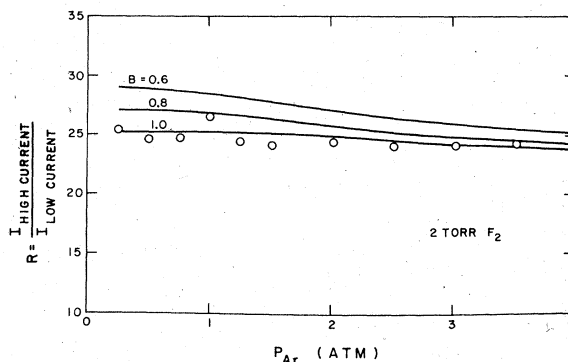


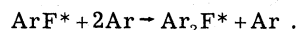
FIG. 5. The measured and calculated ratio of ArF^* fluorescence intensities when the E -beam current is changed by a factor of 25. The points are experimental. The three curves are the calculated ratios for branching ratios of 1, 0.8, and 0.6.

increasing Ar pressure is caused by quenching of ArF^* by Ar. So the ArF^* fluorescence signal S can be written as

$$S = \frac{\alpha N_{\text{Ar}}}{1 + (k_{\text{F}_2} N_{\text{F}_2} + k_{\text{Ar}} N_{\text{Ar}} + k_{2\text{Ar}} N_{\text{Ar}}^2) \tau}, \quad (1)$$

where α is a constant, τ is the ArF^* radiative lifetime, k_{F_2} is the quenching-rate constant of ArF^* by F_2 , and k_{Ar} and $k_{2\text{Ar}}$ are the two- and three-body quenching-rate constants of ArF^* by Ar. N_{F_2} and N_{Ar} are the number densities of F_2 and Ar, respectively. We have ignored the three-body quenching of ArF^* by F_2 because of the low concentration (2 torr) of F_2 used. For example, a three-body rate constant of 10^{-30} cm⁶/sec for F_2 would change the results by $\leq 10\%$. Analysis of Eq. (1) to obtain the $k\tau$ products has been discussed in detail previously.⁸ The curve in Fig. 4 is a plot of Eq. (1) using the quenching-rate constants obtained by that analysis.

Figure 6 shows the Ar_2F^* fluorescence amplitude as a function of Ar pressure. Since ArF^* is formed first, we postulate that Ar_2F^* is formed by the following reaction:



As evidence of this thesis, the shape of the Ar_2F^* fluorescence amplitude versus Ar pressure has been calculated assuming ArF^* is formed first and subsequently recombines with Ar to form Ar_2F^* . The result of this calculation is shown as the solid curve plotted in Fig. 6. The deviation of the experimental data from the curve at high pressures is probably due to the quenching of Ar_2F^* by Ar.

C. Displacement reaction

The rate constant for the displacement reaction $\text{Kr} + \text{ArF}^* \rightarrow \text{KrF}^* + \text{Ar}$ was obtained by observing

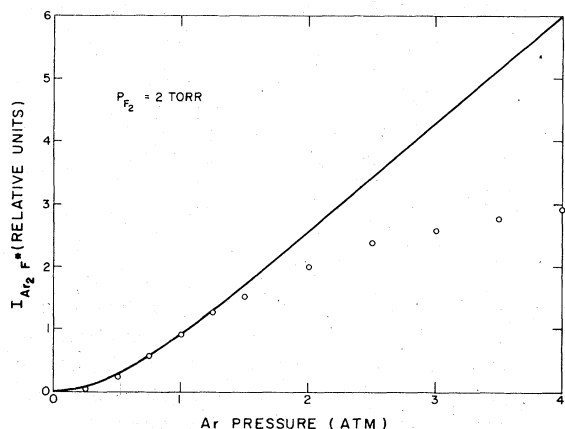


FIG. 6. The Ar_2F^* fluorescence in the presence of 2-torr F_2 as a function of Ar partial pressure. The curve is the predicted Ar_2F^* fluorescence for negligible quenching of Ar_2F^* .

the decay of the steady-state fluorescence intensity at 1930 Å as the partial pressure of Kr was increased. These measurements were made in mixes containing a constant amount of Ar and F_2 . The argon partial pressure was 100 torr to minimize the formation of Ar_2^+ (see Fig. 2). In fact, at this low pressure and for an E -beam current of 5 A/cm² we have numerically evaluated that the density of Ar^+ is about an order of magnitude greater than that of Ar_2^+ . Figure 7 shows the predicted decays of ArF^* for our experimental conditions for two cases: (i) ignoring the Ar^+ channel and (ii) including the Ar_2^+ channel; the Ar_2^+ channel introduces a variation of about 10% in this comparison. Figure 8 shows a Stern-Volmer plot of the ArF^*

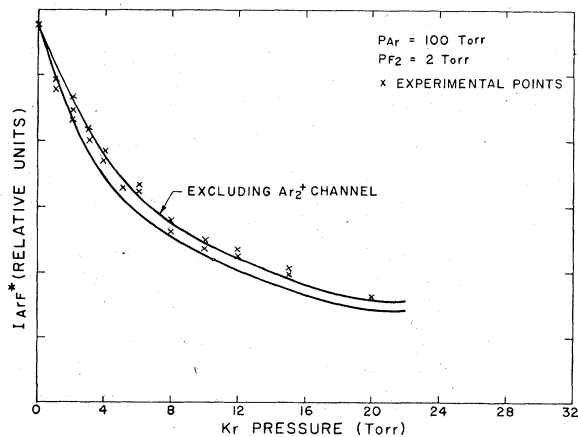


FIG. 7. The predicted and measured ArF^* fluorescence as a function of the Kr partial pressure. When the charge transfer channel is excluded, the predicted decay of the ArF^* signal as a function of Kr pressure is about 10% slower.

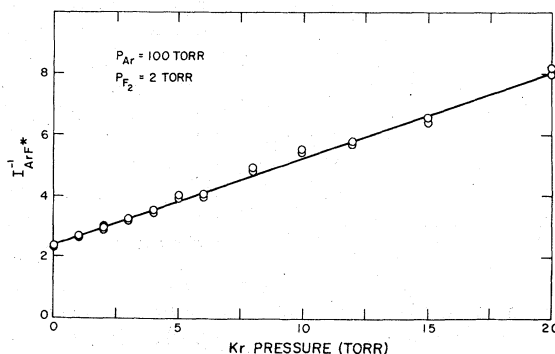


FIG. 8. Stern-Volmer quenching curve for ArF^* with Kr.

fluorescence data as a function of the Kr partial pressure. From these plots we obtain the half quenching pressure of ArF^* by Kr. The displacement-reaction rate constant was also measured by observing the increase in the KrF^* fluorescence amplitude with increasing Kr partial pressure. This measurement gives the same rate constant to within 10%, so one can conclude that Kr displaces ArF^* to form KrF^* with a branching ratio near unity.

The radiative lifetime of ArF^* has been calculated to be 4 ns by Dunning and Hay.¹⁵ Such a short lifetime gives a displacement rate constant ($\text{Kr} + \text{ArF}^* \rightarrow \text{KrF}^* + \text{Ar}$) of $1.6 \times 10^{-9} \text{ cm}^3$. This rate constant seems unusually large even for this sort of reaction. For example, the kinetically similar alkali-halide reaction $\text{Rb} + \text{KF} \rightarrow \text{RbF} + \text{K}$ has a rate constant about an order of magnitude smaller than these rare-gas halide displacement reactions.¹⁶ One reason for the difference may be related to the much higher exothermicity of the rare-gas halide displacement reactions.¹⁷ Another possible explanation for the rapid displacement-rate constant is that at low pressure, the Kr atom displaces the Ar atom when the ArF^* is in a high vibrational level and thus has a large cross section. At higher pressures the vibrational relaxation of ArF^* will proceed more rapidly. Therefore, one might expect the measured displacement rate to decrease with increasing pressure. Preliminary measurements at 200- and 300-torr Ar indicates that this indeed may be the case.

IV. FORMATION AND QUENCHING OF KrF^*

A. Formation of KrF^*

In mixtures containing mainly Ar at low total pressures, ArF^* is formed first. KrF^* is subsequently formed by the displacement reaction as discussed in the previous section. At pressures of about 1 atm and greater (depending on E -beam

TABLE III. Dominant quenching processes of KrF*.

Reaction	$k\tau_R(\text{KrF}^*)$	$k(\tau_R = 6.5 \text{ nsec})$	
$\text{KrF}^* + \text{F}_2 \rightarrow \text{Products}$	$5 \times 10^{-18} \text{ cm}^3$	$7.8 \times 10^{-10} \text{ cm}^3 \text{ sec}^{-1}$	(1)
$\text{KrF}^* + 2\text{Kr} \rightarrow \text{Kr}_2\text{F}^* + \text{Kr}$	$4.4 \times 10^{-39} \text{ cm}^6$	$6.7 \times 10^{-31} \text{ cm}^6 \text{ sec}^{-1}$	(2)
$\text{KrF}^* + \text{Kr} \rightarrow \text{Products}$	$\leq 1.1 \times 10^{-20} \text{ cm}^3$		(3)
$\text{KrF}^* + \text{Kr} + \text{Ar} \rightarrow \text{Kr}_2\text{F}^* + \text{Ar}$	$4.2 \times 10^{-39} \text{ cm}^6$	$6.5 \times 10^{-31} \text{ cm}^6 \text{ sec}^{-1}$	(4)
$\text{KrF}^* + 2\text{Ar} \rightarrow \text{Products}$	$4.6 \times 10^{-40} \text{ cm}^6$	$7 \times 10^{-32} \text{ cm}^6 \text{ sec}^{-1}$	(5)

current density), molecular argon-ion formation becomes important. The Ar_2^+ rapidly charge transfers with Kr to form Kr^+ .¹⁸ For lean Kr mixes the Kr^+ recombines with F^- to form KrF^* . As the Kr partial pressure and total mixture pressure are increased, Kr_2^+ will be formed. By experimental measurements similar to those discussed in the previous section, we have shown that Kr_2^+ recombines with F^- to form mainly KrF^* . Once KrF^* is formed it can radiate or be quenched by the constituents of the gas mixture. The dominant quenching processes and reaction rates are listed in Table III.

B. Quenching of KrF*

The rate constant for quenching of KrF^* by F_2 was measured by observing the KrF^* fluorescence amplitude versus pressure in binary mixtures of Kr and F_2 . The procedure was similar to the measurements of ArF^* quenching by F_2 described in the previous section. The two-body quenching of KrF^* by Kr and the three-body quenching by 2Kr were studied in Kr/ F_2 mixes, similar to the analogous case of ArF^* quenching by Ar as discussed in the previous section.

Figure 9 shows the spontaneous emission spectra in mixtures containing 0.3% F_2 , 6% Kr, and 93.7% Ar at various total pressures. The uncalibrated spectral-intensity scale is approximately logarithmic. At 0.5 atm essentially all of the radiation from the mixture is contained in the $\text{KrF}^* \ ^2\Sigma_{1/2} - ^2\Sigma_{1/2}$ band at 248 nm. However, two other broad bands, containing much less energy, are observable. The first is centered at 415 nm and has been identified with the $^2B_2 - A_1$ transition of the excited triatomic Kr_2F^* .¹⁹ The other broad band, centered roughly at 270–280 nm, is most likely a combination of radiation from the $^2\Sigma - ^2\Pi$ band of KrF^* and perhaps radiation from the excited triatomics Ar_2F^* ¹⁸ and ArKrF^* . Identification of the Kr_2F^* and Ar_2F^* ²⁰ bands was inferred by observing the radiation from binary mixtures of Ar/ F_2 and Kr/ F_2 . From the Kr/ F_2 mix we observed the same spectra except that some of the structure in the band centered at 270–280 nm disappeared. From the Ar/ F_2 mixture, the spectra showed only a very broad

band centered at 290–300 nm which has been identified as Ar_2F^* radiation. The spectrum obtained at a total mixture pressure of 4 atm indicates that, compared with the 0.5 atm spectrum, essentially the same energy is contained in the $\text{KrF}^* \ ^2\Sigma_{1/2} - ^2\Sigma_{1/2}$ band, although the electron-beam energy deposited increased by a factor of ~8. This spectrum indicates that most of the additional energy deposited by the E beam was channeled to Kr_2F^* . This decrease in the KrF^* fluorescence efficiency and increase in the Kr_2F^* fluorescence efficiency could be due to two possible effects: (i) KrF^* quenching by Ar and Kr or (ii) decreasing formation efficiency of KrF^* . Such a decrease is expected if Kr_2^+ recombines with F^- to form KrF^* with a branching ratio < 1 . Experiments performed with different E-beam currents, similar to those discussed in the previous section, show that Kr_2^+ recombines with F^- to form KrF^* with a branching ratio near unity.

To further substantiate this conclusion, an ex-

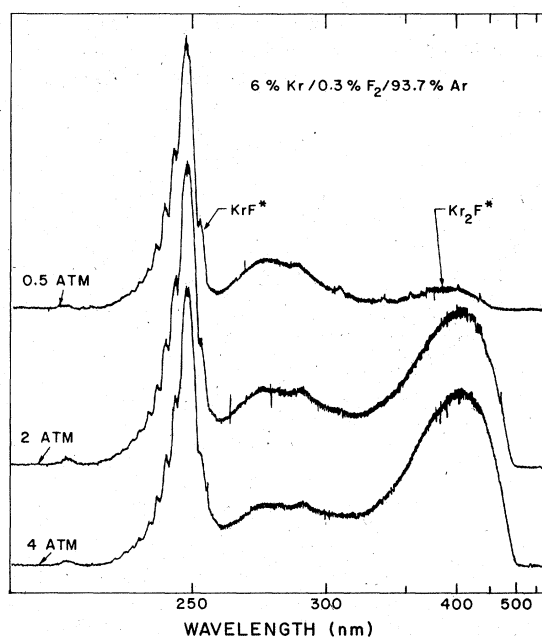


FIG. 9. Spectra of a 6% Kr mixture at various total pressures.

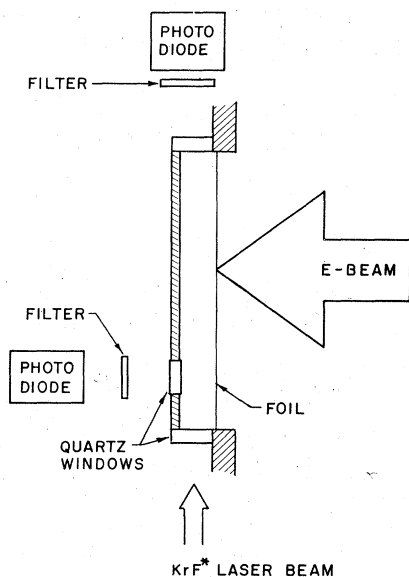


FIG. 10. Experimental setup for the KrF^* and Kr_2F^* saturation experiments.

periment was performed in which some of the KrF^* molecules formed were deactivated by stimulated transition induced by a KrF^* laser before they could be collisionally quenched. If Kr_2F^* is formed by the quenching of KrF^* as our measurements indicate, then stimulation of the KrF^* transition ($B^2\Sigma_{1/2} - X^2\Sigma_{1/2}$) by intense radiation at 249 nm should lead to a decrease in the Kr_2F^* fluorescence amplitude. The experimental setup for the measurement is shown in Fig. 10. Radiation from a KrF^* transversely excited (TEA) laser was transmitted along the length of the cell containing a KrF^* laser mixture. The sidelight emission at the 249-nm band (KrF^*) and at 410 nm (Kr_2F^*) were monitored by photodiodes with appropriate filters. The results of these measurements are shown in Fig. 11. Figures 11(a) and 11(b) display the KrF^* and Kr_2F^* sidelight fluorescence upon introduction of the KrF^* laser pulse. Figure 11 (c) shows the Kr_2F^* sidelight fluorescence when no KrF^* laser radiation is present. The results of this set of experiments confirm that Kr_2F^* is a product of the KrF^* quenching. Therefore, the decrease of the KrF^* fluorescence efficiency with increasing pressure is a result of quenching by Ar and Kr.

The quenching of KrF^* by processes (4) and (5) in Table III were studied in Ar/Kr/ F_2 mixtures. Reaction (5) was determined by analyzing the dependence of the KrF^* fluorescence on the Ar partial pressure. The F_2 and Kr partial pressures were kept constant for these runs. For such a mix, reaction (4) appears as an effective two-body re-

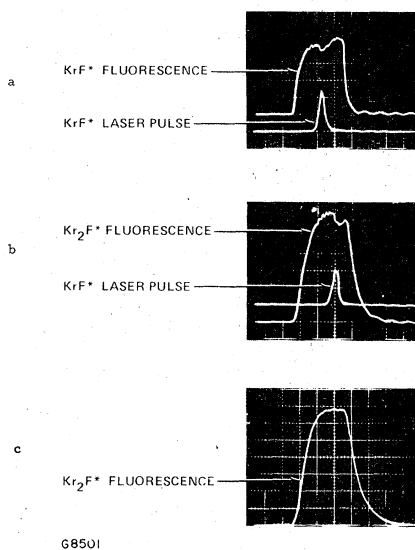


FIG. 11. Data showing the KrF^* and Kr_2F^* fluorescence in the presence of KrF^* laser radiation. The bottom oscillogram is the Kr_2F^* fluorescence when there is no laser radiation present.

action (Kr constant). Because of their different pressure dependences, two- and three-body processes can be differentiated by an analysis similar to that discussed in detail in Ref. 8.

To measure reaction (4) more accurately, the KrF^* fluorescence intensity as a function of the Kr partial pressure was measured. In these measurements the Ar and F_2 partial pressures were kept constant. Figure 12 shows typical data for the KrF^* fluorescence intensity as a function of Ar partial pressure. The curves represent the predicted pressure dependence of the KrF^* intensity using the rate constants in Table III.

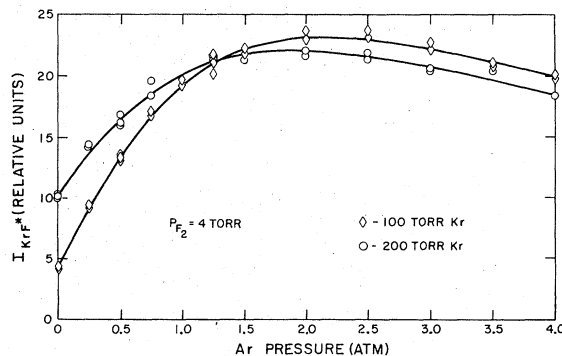


FIG. 12. KrF^* fluorescence signal for Ar/Kr/ F_2 mixtures containing 4-torr F_2 and 100- and 200-torr Kr. The data was taken varying only the Ar partial pressure. The curves are the calculated fluorescence using the rate constants listed in Table III.

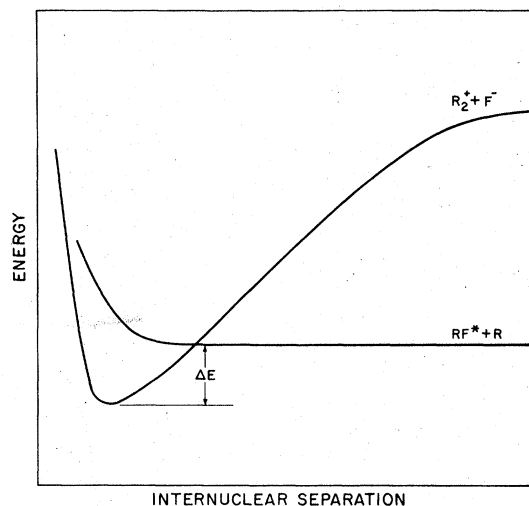


FIG. 13. Schematic of potential curves of $R_2^+ + F^-$ and $RF^* + R$.

V. CONCLUSION

In the preceding sections we have shown that the ArF^* and KrF^* exciplexes can be formed via the ion channel with unit branching. From our measurements we can conclude that the decrease of the fluorescence intensity with increasing pressure is a result of two- and three-body quenching of the exciplex.

Interception of the precursors (Ar^+ , Kr^+ , and F^-) of these exciplexes are a negligibly small effect when the experimental conditions are chosen properly. In a laser it is possible to minimize the

loss due to the quenching processes by saturating the lasing transition. From the spontaneous emission spectra and the measured quenching-rate constants, the saturation flux can be calculated for a particular mixture. This information, coupled with the knowledge of the photoabsorption of the active medium, can be used to optimize laser mixes. The dominant quenching processes of ArF^* ($B^2\Sigma_{1/2}$) and KrF^* ($B^2\Sigma_{1/2}$) have been identified and their rate constants have been measured. The only important two-body quenching is due to F_2 . Three-body quenching by the rare gases becomes important at pressures above 1 atm. These quenching processes result in the formation of excited triatomics Ar_2F^* and Kr_2F^* .

The formation of the excited triatomics can be understood by looking at the schematic potential curves shown in Fig. 13. The rare gas R approaches the rare-gas fluoride RF^* on a repulsive curve that intersects the $R_2^+F^-$ potential curve. The surface of the interaction will be dependent on ΔE , the exothermicity of the interaction. The larger ΔE , the larger the surface area, and hence the interaction will proceed with a higher probability. According to the calculation of Wadt and Hays¹⁴ $\Delta E \approx 0.6$ eV for Ar_2F^* and Kr_2F^* . For Xe_2F^* , ΔE is only 0.2 eV. This small exothermicity might be responsible for the fact that Xe_2F^* has not been observed.

ACKNOWLEDGMENT

We greatly appreciate the expert technical assistance of R. Brochu.

†This research was supported by the Advanced Research Projects Agency and monitored by the Office of Naval Research under Contract No. N00014-75-C-0062.

‡On leave from Hebrew University of Jerusalem, Israel.

¹This term is strictly more appropriate than excimer for excited rare-gas halides since they are composed of two different species. In contrast, the term "excimer" is derived from "excited dimer," where dimer implies a joining of two of the same species.

²J. E. Velazco and D. W. Setser, *J. Quant. Electron.* **11**, 708-709 (1975).

³J. J. Ewing and C. A. Brau, *Appl. Phys. Lett.* **27**, 350-352 (1975); C. A. Brau and J. J. Ewing, *Appl. Phys. Lett.* **27**, 435-437 (1975); S. K. Searles and G. A. Hart, *Appl. Phys. Lett.* **27**, 243-245 (1975); E. R. Ault, R. S. Bradford, and M. L. Bhaumik, *Appl. Phys. Lett.* **27**, 413-415 (1975).

⁴J. A. Mangano and J. H. Jacob, *Appl. Phys. Lett.* **27**, 495-497 (1975); R. Burnham, H. W. Harris, and N. Djeu, *Appl. Phys. Lett.* **28**, 86-87 (1976); C. P. Wang, H. Mirels, D. G. Sutton, and S. N. Suchard,

Appl. Phys. Lett. **28**, 326-328 (1976); J. A. Mangano, J. H. Jacob, and J. B. Dodge, *Appl. Phys. Lett.* **29**, 426-428 (1976).

⁵J. A. Mangano *et al.* (unpublished).

⁶R. Hunter (unpublished).

⁷J. E. Velazco, J. H. Kolts, and D. W. Setser, *J. Chem. Phys.* **65**, 3468-3485 (1976).

⁸M. Rokni, J. H. Jacob, J. A. Mangano, and R. Brochu, *Appl. Phys. Lett.* **30**, 458-460 (1977).

⁹L. R. Peterson and J. E. Allen, Jr., *J. Chem. Phys.* **56**, 6068-6076 (1972).

¹⁰M. Rokni, J. H. Jacob, J. A. Mangano and R. Brochu, *Appl. Phys. Lett.* **31**, 79 (1977).

¹¹M. R. Flannery (unpublished).

¹²It was determined *a posteriori* that at 150 torr the Ar quenching of ArF^* introduces a 5% error. This error was corrected for subsequently.

¹³By branching ratio we mean the fraction of Ar_2^+ that forms ArF^* .

¹⁴W. R. Wadt and P. J. Hay, *Appl. Phys. Lett.* **30**, 573-575 (1977).

¹⁵T. H. Dunning and P. J. Hay, *Appl. Phys. Lett.* **28**,

- 649-651 (1976).
- ¹⁶S. Stolte, A. E. Proctor, and R. B. Bernstein, *J. Chem. Phys.* **65**, 4990 (1976).
- ¹⁷M. Krauss, Natl. Bur. Stand. (private communication).
- ¹⁸D. K. Bohme, N. G. Adams, M. Moselman, D. B. Dun-kin, and E. E. Ferguson, *J. Chem. Phys.* **52**, 5094 (1970).
- ¹⁹J. A. Mangano, J. H. Jacob, M. Rokni, and A. Hawry-luk, *Appl. Phys. Lett.* **31**, 26 (1977).
- ²⁰M. Krauss, Natl. Bur. Stand. (private communication).
- ²¹H. L. Chen, R. E. Center, D. W. Trainor, and W. I. Fyfe, *Appl. Phys. Lett.* **30**, 99 (1977).
- ²²E. W. McDaniel, V. Cermak, A. Dalgarno, E. E. Fer-guson, and L. Friedman, *Ion-Molecule Reactions* (Wiley-Interscience, New York, 1970), pp. 338-339.

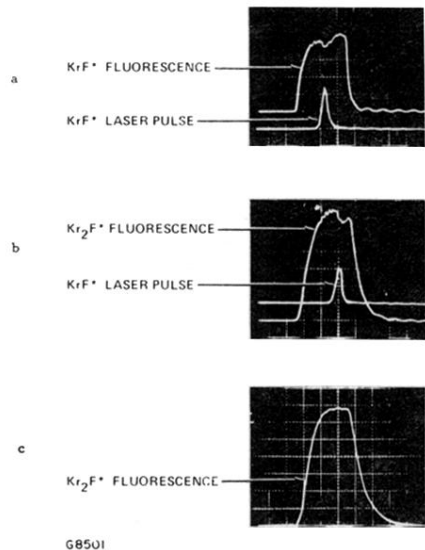


FIG. 11. Data showing the KrF* and Kr₂F* fluorescence in the presence of KrF* laser radiation. The bottom oscillogram is the Kr₂F* fluorescence when there is no laser radiation present.